



**HAL**  
open science

## Subthalamic Nucleus Location: Relationships between Stereotactic AC-PC-Based Diagrams and MRI Anatomy-Based Contours

François Caire, Lemlih Ouchchane, Jerome Coste, Jean Gabrillargues, Philippe Derost, Miguel Ulla, Franck Durif, Jean-Jacques Lemaire

► **To cite this version:**

François Caire, Lemlih Ouchchane, Jerome Coste, Jean Gabrillargues, Philippe Derost, et al.. Subthalamic Nucleus Location: Relationships between Stereotactic AC-PC-Based Diagrams and MRI Anatomy-Based Contours. *Stereotactic and Functional Neurosurgery*, 2009, 87, pp.337 - 347. 10.1159/000236367 . hal-01552987

**HAL Id: hal-01552987**

**<https://uca.hal.science/hal-01552987>**

Submitted on 3 Jul 2017

**HAL** is a multi-disciplinary open access archive for the deposit and dissemination of scientific research documents, whether they are published or not. The documents may come from teaching and research institutions in France or abroad, or from public or private research centers.

L'archive ouverte pluridisciplinaire **HAL**, est destinée au dépôt et à la diffusion de documents scientifiques de niveau recherche, publiés ou non, émanant des établissements d'enseignement et de recherche français ou étrangers, des laboratoires publics ou privés.

Subthalamic Nucleus Location:  
Relationships between Stereotactic AC-PC-Based Diagrams  
and MRI Anatomy-Based Contours

François CAIRE<sup>(1, 2,\*)</sup>, Lemlih OUCHCHANE<sup>(1, 4)</sup>, Jérôme COSTE<sup>(1, 3)</sup>,  
Jean GABRILLARGUES<sup>(1,5)</sup>, Philippe DEROST<sup>(6)</sup>, Miguel ULLA<sup>(6)</sup>, Franck DURIF<sup>(6)</sup>,  
Jean-Jacques LEMAIRE<sup>(1, 3)</sup>

(1) *Équipe de Recherche en Imagerie Médicale, ERIM-EA 3295. ERI 14 ESPRI/INSERM, Université d'Auvergne, Clermont-Ferrand.*

(2) *Service de Neurochirurgie, CHU Limoges, Hôpital Dupuytren, 87042 Limoges.*

(3) *Service de Neurochirurgie A ; (4) Service de Biostatistiques ; (5) Service de radiologie A, unité de neuro-radiologie*

*et (6) Service de Neurologie A, Hôpital Gabriel-Montpied, CHU de Clermont-Ferrand, BP 69, 63003 Clermont-Ferrand Cedex 1.*

(\*) *Auteur correspondant : François Caire, Service de Neurochirurgie, Hôpital Dupuytren, CHU de Limoges, 2, avenue Martin Luther King, FR-87042 LIMOGES, FRANCE; francois.caire@chu-limoges.fr*

## ABSTRACT

Subthalamic nucleus (STN) targeting is classically performed based on AC-PC probabilistic position. Nevertheless, MRI allows direct visualization and targeting. We aimed to compare the position localized on MR images with standard stereotactic diagrams. The STN was manually contoured on MR images (22 Parkinson's disease patients); boundaries were simplified in a schematic polygonal form. Front and lateral stereotactic diagrams were constructed according to Talairach and Benabid. We compared x, y and z coordinates of the geometrical center of MRI-based polygons and stereotactic diagrams (Wilcoxon matched-pairs tests). There was significant discordance between MRI-based polygons and AC-PCbased images. MRI shows the STN as more posterior, medial and slightly inferior.

## KEY WORDS

Subthalamic nucleus targeting, Deep brain stimulation, Stereotactic AC-PC-based diagrams

## INTRODUCTION

In stereotactic surgery, anatomical or ‘primary’ targeting of the subthalamic nucleus (STN) can be performed using two different approaches.

The classical method, called ‘indirect targeting’, is based on determining geometric coordinates of a so-called target, in this case the STN. Theoretically, any target can be defined in a stereotactic space oriented by third-ventricle landmarks (anterior commissure, AC; posterior commissure, PC, and possibly thalamus height, TH) defining the AC-PC orientation and subsequently the axis: (a) laterality along the x-axis on both sides of the vertical AC-PC plane; (b) anterior-posterior direction along the y-axis, the AC-PC line (anterior, positive; posterior, negative; the reference point is often the PC or the mid-commissural point, MidP); (c) superior-inferior direction, or depth, along the z-axis above (positive) or below (negative) the horizontal AC-PC plane. Landmarks historically localized via ventriculography are now localized by magnetic resonance imaging (MRI). Stereotactic AC-PC-based diagrams show the position of the STN within the stereotactic space [1, 2]. Stereotactic diagrams were historically constructed on projection imaging (Xrays), thus giving front and lateral views. STN diagrams represent an average location of the anatomic structure, supposed to integrate interindividual variability determined by anatomical [1] and/or clinical [2] studies, making STN targeting essentially ‘probabilistic’. Intraoperative assessments (clinical tests, microrecordings) are required to fit the positioning of the contact electrode (deep brain stimulation, DBS) or lesion to the clinical aims, in a phase called secondary targeting. Stereotactic atlases like the Schaltenbrand and Bailey atlas [3] are also helpful for indirect targeting; STN location is usually identified on microscopic slices although macroscopic slices including probabilistic areas are also available. Despite well-known limitations related to sections of the anatomic specimen, stereotactic atlases are still used worldwide. Deformable atlases [4–7] have been introduced to match patient images to atlas images with a certain degree of proportionality. Advances in MRI have also led teams to propose the red nucleus as local stereotactic reference for indirect STN targeting [8].

The second method for primary targeting is called ‘direct targeting’. It is based on spontaneous contrasts between white (WM) and gray (GM) matter with appropriate sequences delineating STN contours (for an overview, see Lemaire et al. [ 9 ]). The advantage is that referencing to internal landmarks is no longer mandatory because there is no need for atlases or diagrams. The

drawbacks stem rather from issues involving anatomical knowledge and, obviously, high-quality images.

Direct or indirect primary targeting can be used indifferently, alone or mixed, depending on surgical environment (technology, habits), institutional and/or national rules on quality assurance, and professional guidelines.

The relationships between STN stereotactic diagrams and MRI anatomy must be explored using a reference imaging procedure, i.e., the one used by the surgical team for primary targeting: stereotactic diagrams or MRI anatomy. Publications using indirect primary targeting as reference procedure [8, 10] have reported that indirect STN targeting is more relevant for DBS electrode placement. This conclusion must be weighed against the methods used. If the reference procedure for primary targeting is indirect, then secondary targeting is performed accordingly, and even if it does slightly adjust the location (usually at worst on a second tract within 2 mm around the tract used for primary targeting), the final location is *de facto* close to the indirect primary-targeted area. Moreover, retrospective analysis of indirect primary targeting versus MRI direct STN imaging according to the contact location providing the best clinical results [8, 10] only highlights differences between final electrode position and primary indirectly targeted area or MRI STN location. The conclusion would rather be that (primary plus secondary) indirect targeting allows a good placement of electrode contact but that does not fit well with the MRI STN anatomy. Cuny et al. [11], in 2002, found the same results comparing postoperative location of contacts (without analysis of clinical results). If we deduce that the AC-PC-based STN target does not represent the exact STN location, it becomes clear that the best clinical target is rather outlying located at the superior and lateral border of the STN and/or zona incerta and Forel's field, as reported by numerous teams using indirect or direct primary targeting [12–18]. These data are confirmed by postmortem studies showing that effective contacts can be located in the zona incerta and Forel's field (for a review, see McClelland et al. [19] and Sun et al. [20]).

For this study, we used MRI anatomy as reference procedure since our institution has been routinely performing a direct targeting technique since 1999 [21, 22]. We compared two kinds of STN localization projected on both frontal and lateral views: (a) stereotactic diagrams constructed according to the classical indirect method; (b) MRI anatomy-based polygons constructed according to STN contours identified visually on MRI. For all subjects, diagrams and

polygons were referenced into the same AC-PC stereotactic space to enable analysis of concordance between diagrams and polygons. Imaging data (1.5-tesla, stereotactic MRI, i.e., stereotactic frame in place) came from a group of patients operated on in our institution, and the images have been anonymized for further analysis.

## MATERIALS AND METHODS

### SUBJECTS

Imaging datasets came from 22 patients, aged 60 +/-6 years (mean +/- standard deviation, SD) and suffering from severe Parkinson's disease. All patients benefited from DBS surgery with bilateral electrode implantation in the subthalamic region giving good clinical results: mean improvement 3 months after surgery was 68% (55–88%) for the UPDRS-III (Unified Parkinson's Disease Rating Scale) subscore and 68% (30–100%) for the UPDRS IV subscore.

### MRI DATASETS

Preoperative stereotactic (stereotactic frame in place, parallel to the cranial base; Leksell-G frame; Elekta Instruments, Sweden) MRI was performed using routine clinical conditions on a 1.5-tesla imaging unit (Sonata; Siemens, Germany). Imaging parameters were as follows: T2-weighting, turbo spin echo (TSE) sequence, coronal plane, echo time = 8 ms, repetition time = 8,000 ms, 24 contiguous slices, field of view = 280 mm, final voxel size = 0.6 x 0.5 x 2 mm<sup>3</sup>. A total number of 528 slices were used for further analysis (22 datasets x 24 images).

### STN CONTOURING ON MRI

Right and left STN were contoured on native (without interpolated display) coronal images ( fig. 1 ), based on the consensus of two physicians (J.J.L. and F.C.) fully conversant with dedicated stereotactic software (iPlan; BrainLAB, Germany) and possessing advanced anatomical knowledge of the subthalamic region. We looked for STN boundaries using spontaneous

WM/GM contrasts following a procedure detailed elsewhere [9]. Briefly, with the T2-weighted TSE sequence, the GM of the STN, thalamus and substantia nigra (SN) appeared hyperintense. The coronal slice showed that the STN had a pseudo-lenticular shape and laid above the SN and below the thalamus. The boundary between the STN and SN was identified as a triangular hypointense notch in contact with the internal capsule. The largest part of the STN was located anteriorly to the anterior pole of the red nucleus.

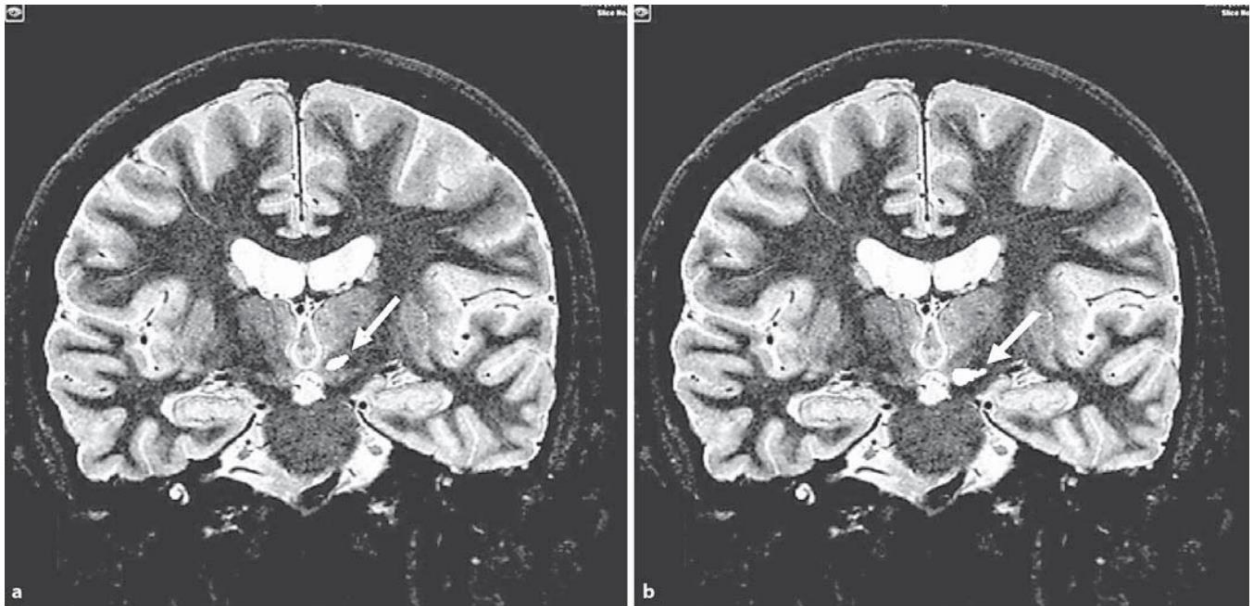


**Figure 1.** STN contouring on coronal T2-weighted MR images. Right STN (a) and substantia nigra (b) are in white (see arrows).

Contouring was realized on all the slices where the STN was visible, allowing 3-dimensional reconstruction. Sagittal reconstructed slices were used for further analysis (see below) and to confirm correct STN location above the SN and below the thalamus and Forel's fields (WM, hypointense) ( fig. 2 ).

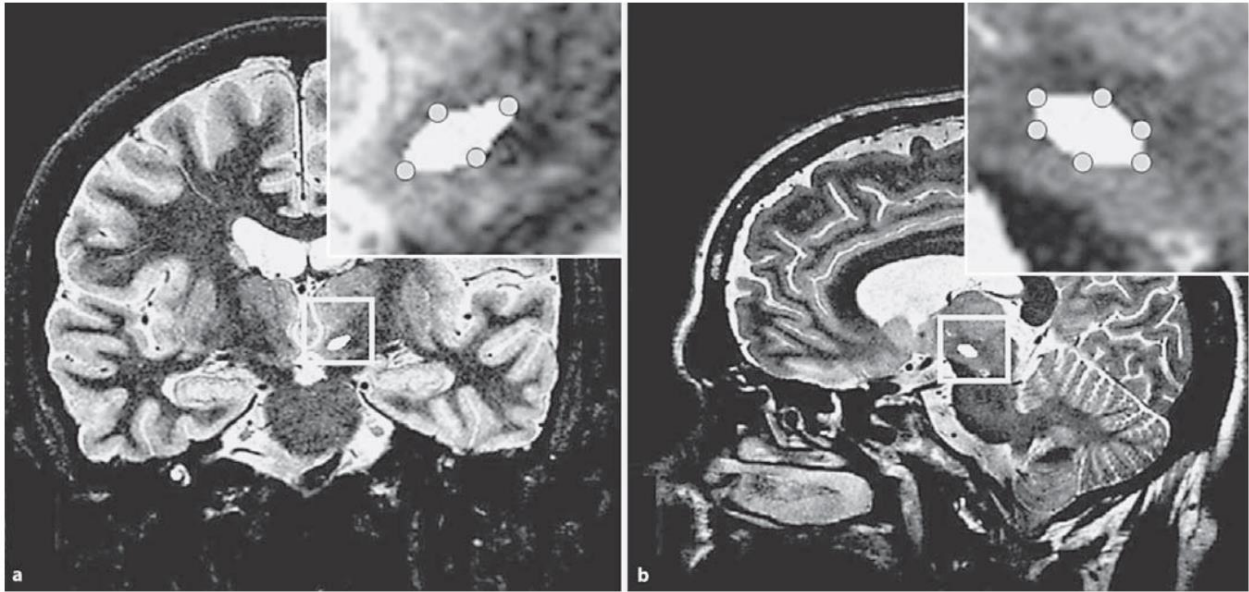


**Figure 2.** Polygonal simplification of STN contouring on a coronal slice (**a**, native MR image) and a sagittal slice (**b**, image reconstructed from the coronal image set). STN contours were simplified as polygons using the same number of points as in stereotactic AC-PC-based diagrams, i.e., 4 points on coronal images (**a**) and 6 on sagittal images (**b**).

### POLYGONAL SIMPLIFICATION OF STN CONTOURS

STN contours were simplified in a schematic polygonal form. The transposition from slice imaging to projections was designed as follows: we selected one STN contour in the slice with the maximally extended nucleus, giving a front view in the coronal plane, and a lateral view in the sagittal plane.

To compare polygons with AC-PC-based stereotactic diagrams, the polygons were constructed using almost the same shape and number of points: front view, 4 points; lateral view, 6 points. The biconvex lens shape of the STN in the coronal slice (front view) enabled diamond-shaped polygonal simplification (main axis oblique lateral and superior; fig. 2 a); in the sagittal slice, the polygonal simplification was hexagonal ( fig. 2 b).

## CONSTRUCTION OF STEREOTACTIC AC-PC-BASED DIAGRAMS

We constructed both Talairach and Benabid diagrams which differ slightly according to ( fig. 3 , 4 ): (a) AC-PC positioning, from the superior AC border to the inferior PC border, and between the AC and PC midpoints; (b) proportionality of the diagram, i.e., relatively partial and less partial.

According to Talairach et al. [1], the lateral diagram is lined above by the AC-PC line and below by the HS line (-4 mm, parallel to AC-PC) and 2 vertical lines perpendicular to the AC-PC (line A, posterior third; line B, anterior third). These 4 lines form a rectangle where the diagonal, from the posterior-inferior to the anterior-superior, defines the main axis of the STN representation. The hexagon representing the STN is formed by the intersection between the rectangle and a 2-mm strip on either side of its main axis. On the front view, the image is lined by the AC-PC and HS and 2 vertical lines parallel to the interhemispheric plane, at 10 and 13 mm laterally. The medial superior corner is withdrawn, cut by a line connecting the lateral superior corner to the midpoint of the opposite vertical line, as shown in figure 3 .

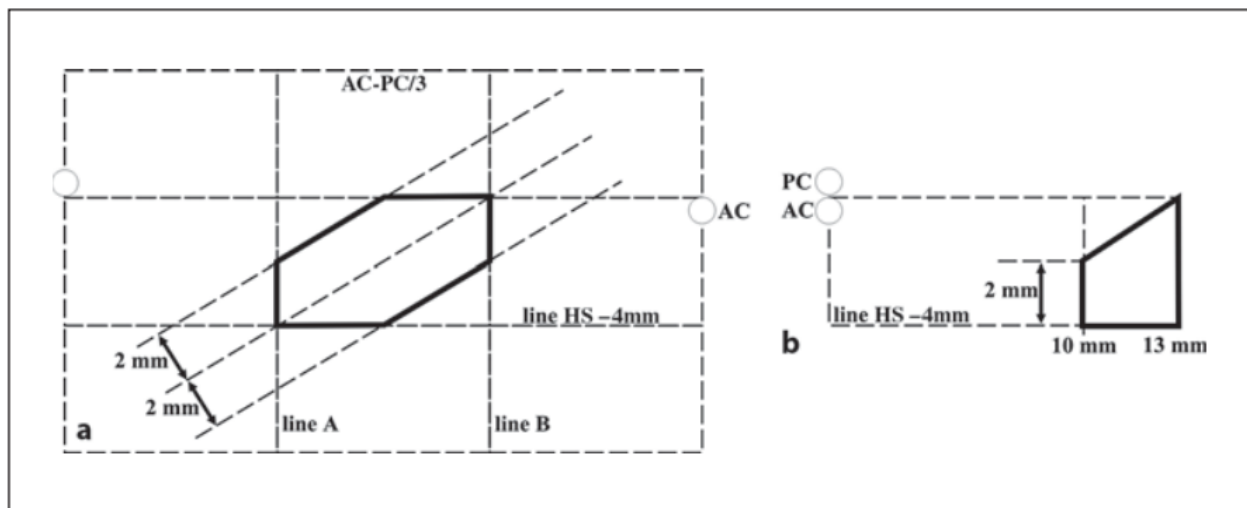


**Figure 3.** Talairach's stereotactic diagram. **a** Lateral. **b** Front.

Benabid et al. [2] provided slightly different diagrams ( fig. 4 ). The line parallel to the AC-PC, below the rectangle, is set at a quarter of the thalamus height ( $TH/4$ , usually slightly above 4 mm). The strip intersecting the rectangle is defined by 2 parallel lines connecting the midpoints of adjacent sides. On the front view, it is similar to Talairach's diagram.

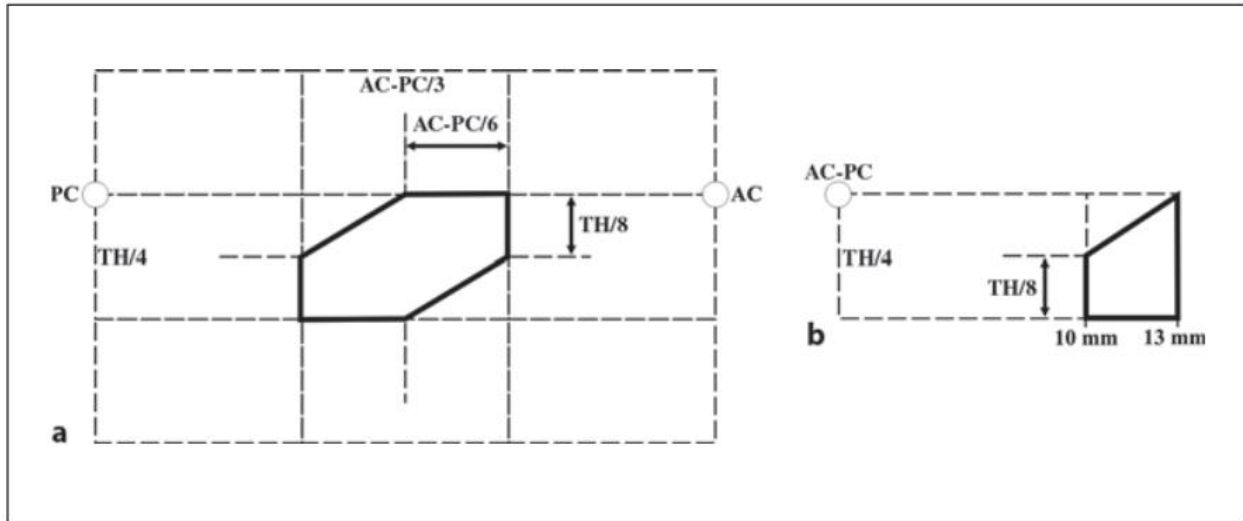


**Figure 4.** Benabid's stereotactic diagram. **a** Lateral. **b** Front.

## COMPARISON OF MRI ANATOMY-BASED POLYGONS AND STEREOTACTIC AC-PC-BASED DIAGRAMS

MRI anatomy-based polygons of the 22 subjects were coregistered on both front and lateral views according to Benabid's and Talairach's diagrams. The coordinates of geometrical centers (CG) of AC-PC-based diagrams and MRI anatomy-based polygons were computed and a discordance test for each CG coordinate ( $x$ ,  $y$  and  $z$ ) was performed using Wilcoxon matched-pairs tests.

For a more convenient analysis of MRI anatomy-based polygons, we proposed a graphic representation making it easy to compare against stereotactic AC-PC-based diagrams. An individual map was created for each subject and on both front and lateral views, dividing the plane into  $0.01\text{-mm}^2$  squares; a value of 1 was allocated to squares within the MRI-based polygon, or a 0 was given otherwise. The 22 individual maps were coregistered and

superimposed, and the mean value of each square was interpreted as a density, creating two density maps – one for the front view and one for the lateral view, where a density of 1 meant that the 22 corresponding squares were included in the MRI anatomybased polygons for the 22 subjects and a density of 0.5 meant that the 22 corresponding squares were included in the MRI anatomybased polygons for 11 subjects. Density maps were displayed using a gray scale from black = 0 or minimum density, to white = 1 or maximum density.

Computations and graphic representations were performed using SAS v9 (SAS Institute Inc., N.C., USA) and MATLAB v7 (The MathWorks, Mass., USA).

## RESULTS

The right and left STN were identified and contoured for all 22 subjects. Mean +/- SD lengths of stereotactic landmarks measured on MRI were: AC-PC = 24.7 +/- 1.57 mm according to Talairach et al. [1], and 24.89 +/- 1.54 mm according to Benabid et al. [2], TH = 16.8 +/- 0.88 mm.

### POLYGONAL SIMPLIFICATION OF STN

The mean 8 SD and range of CG coordinates of MRI anatomy-based polygons were (left and right sides pooled): (1) according to Talairach et al. [1],  $x = 9.04 \pm 1.33$  mm, 6.5–11.6 mm,  $y = 2.82 \pm 0.99$  mm, 7.7–11.8 mm from MidP,  $z$  (on the lateral view) =  $-3.19 \pm 1.01$  mm, -5.9 to -0.5 mm, and  $z$  (on the front view) =  $-2.96 \pm 0.97$  mm, -4.9 to -0.4 mm; (2) according to Benabid et al. [2],  $x = 9.14 \pm 1.3$  mm, 6.5–11.9 mm,  $y = 2.56 \pm 0.96$  mm, 7.75–11.86 mm from MidP,  $z$  (on the lateral view) =  $-3.4 \pm 0.93$  mm, -5.32 to -1.5 mm, and  $z$  (on the front view) =  $-3.18 \pm 0.97$  mm, -5.2 to -1.2 mm.

After normalization in  $y$  by percent AC-PC length and  $z$  by percent TH/4, the mean  $y$  and  $z$  coordinates were: (1) according to Talairach et al. [1],  $y = 0.11 \pm 0.04 \times \text{ACPC}$  ( $z$  values do not change); (2) according to Benabid et al. [2],  $y = 0.1 \pm 0.04 \times \text{AC-PC}$ ,  $z$  (on the lateral view) =  $-0.81 \pm 0.2 \times (\text{TH}/4)$ , and  $z$  (on the front view) =  $-0.76 \pm 0.2 \times (\text{TH}/4)$ .

DISCORDANCE BETWEEN MRI-BASED POLYGONS  
AND STEREOTACTIC AC-PC-BASED DIAGRAMS

Matched-pairs comparisons of CG coordinates between MRI anatomy-based polygons and stereotactic AC-PC-based diagrams revealed a significant difference regarding x ( $p < 0.001$ ), y ( $p < 0.001$ ) and z coordinates ( $p < 0.05$ ) for both right and left STN (results detailed in tables 1 and 2).

| Axis             | Right STN |                      |         | Left STN |                      |         |
|------------------|-----------|----------------------|---------|----------|----------------------|---------|
|                  | polygon   | stereotactic diagram | p value | polygon  | stereotactic diagram | p value |
| x                | 8.9       | 11.5                 | <0.001  | 9.17     | 11.5                 | <0.001  |
| y                | 2.92      | 0                    | <0.001  | 2.72     | 0                    | <0.001  |
| z (front view)   | -2.97     | -2.5                 | <0.05   | -2.94    | -2.5                 | <0.05   |
| z (lateral view) | -3.17     | -2                   | <0.001  | -3.2     | -2                   | <0.001  |

**Table 1.** Comparison of coordinates (in mm) for geometrical centers between MRI anatomy-based polygons and stereotactic AC-PC-based diagrams: Talairach's stereotactic referential space.

| Axis             | Right STN |                      |         | Left STN |                      |         |
|------------------|-----------|----------------------|---------|----------|----------------------|---------|
|                  | polygon   | stereotactic diagram | p value | polygon  | stereotactic diagram | p value |
| x                | 9.08      | 11.5                 | <0.001  | 9.2      | 11.5                 | <0.001  |
| y                | 2.63      | 0                    | <0.001  | 2.5      | 0                    | <0.001  |
| z (front view)   | -3.23     | -2.62                | <0.05   | -3.14    | -2.62                | <0.05   |
| z (lateral view) | -3.5      | -2.1                 | <0.001  | -3.29    | -2.1                 | <0.001  |

**Table 2.** Comparison of coordinates (in mm) for geometrical centers between MRI anatomy-based polygons and stereotactic AC-PC-based diagrams: Benabid's stereotactic referential space.

The density maps showed discordance between the locations of MRI anatomy STN polygons and stereotactic AC-PC-based STN diagrams, regardless of whether the stereotactic reference space was Talairach or Benabid: on the lateral view, MRI anatomy-based polygons were located more inferiorly and posteriorly, whereas on the front view they were located more inferiorly and medially ( fig. 5 , 6 ).

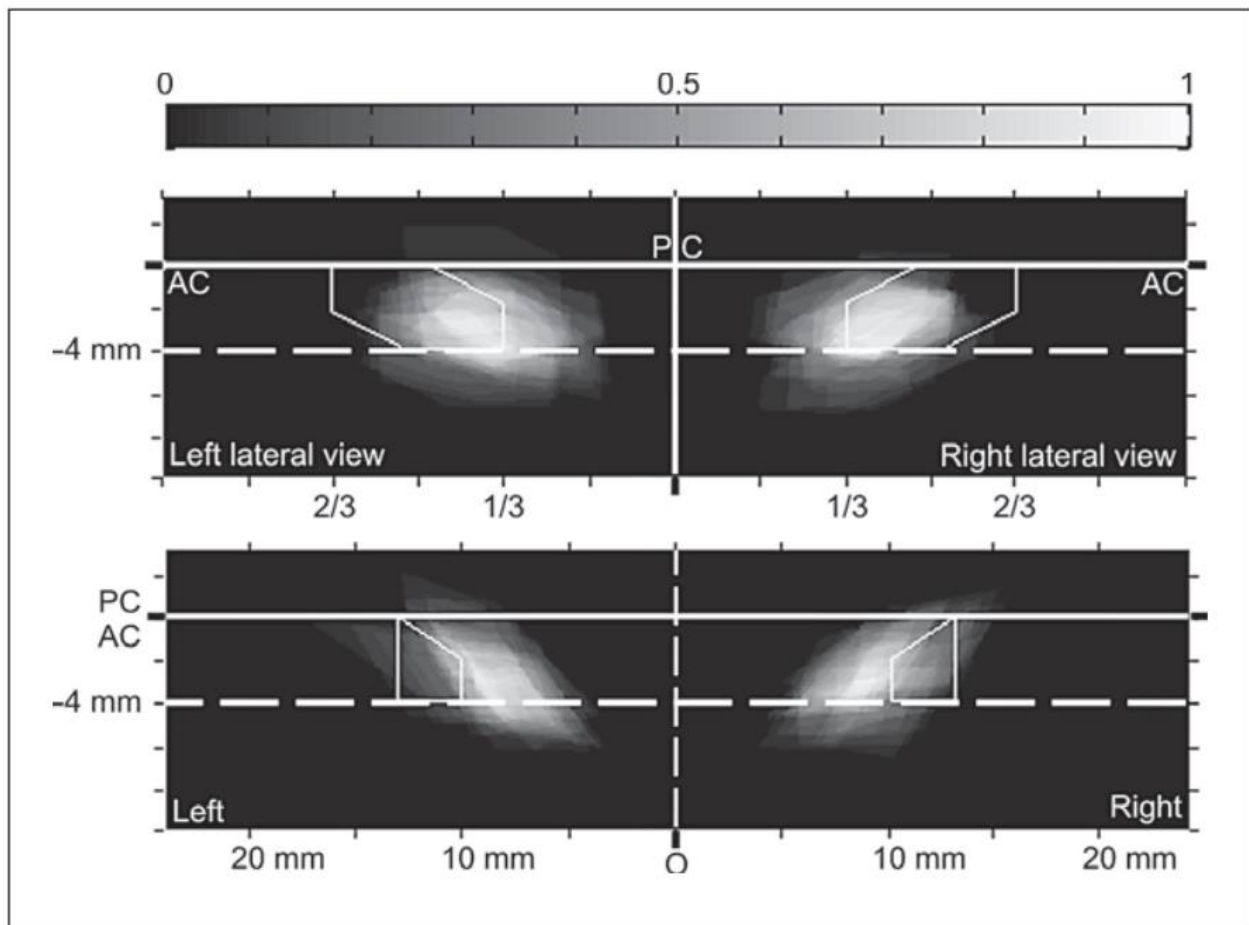


**Figure 5.** Density maps for the lateral (top) and front (bottom) views in Talairach's stereotactic reference space. The plane is divided into  $0.01\text{-mm}^2$  squares, and 22 individual maps are superimposed. A density of 1 means that the 22 corresponding squares are included in the MRI anatomy-based polygons for all the 22 subjects. A density of 0.5 means that the corresponding

squares were included in the MRI anatomy-based polygons for 11 subjects. Density maps are displayed using grayscale from black = 0 to white = 1.

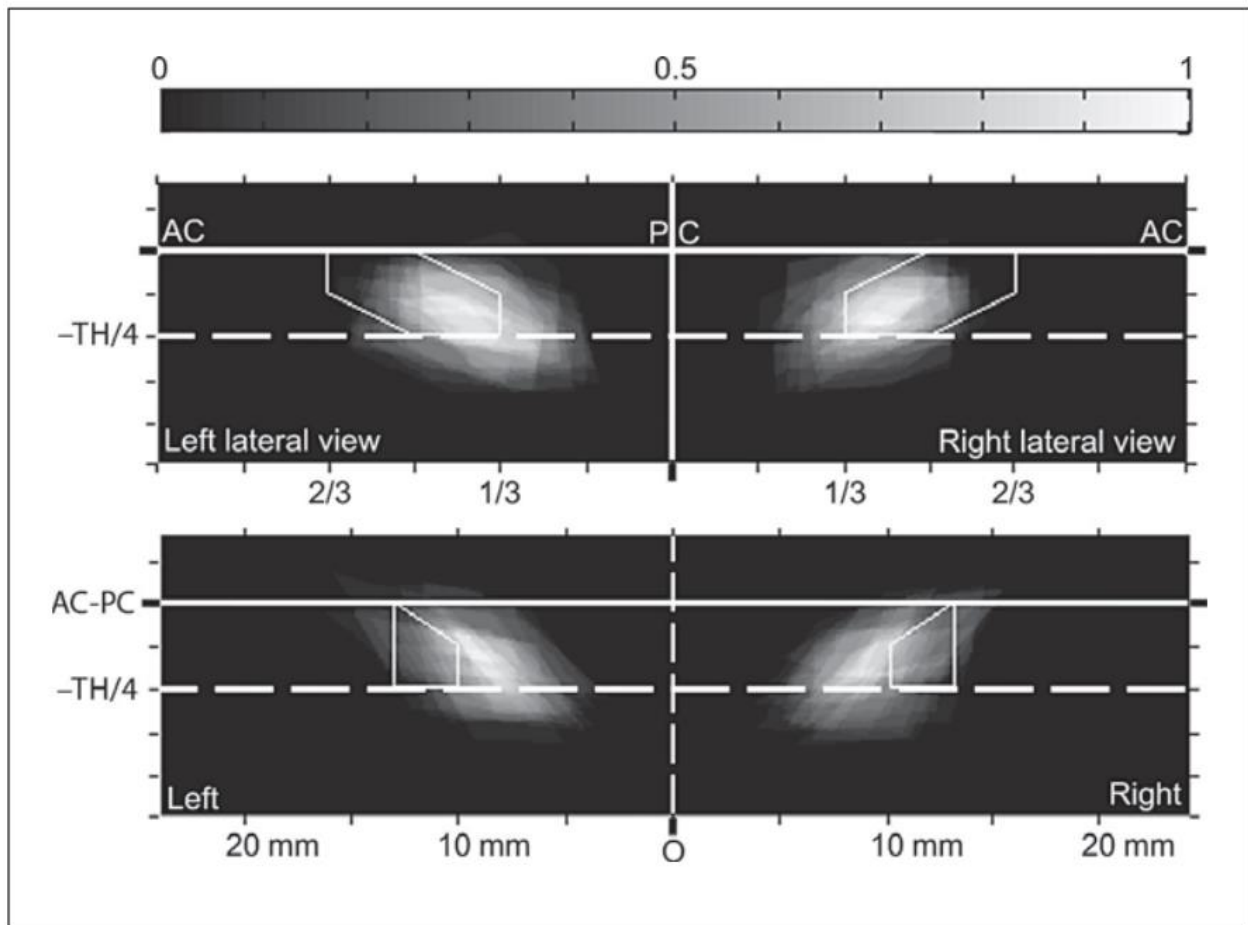


**Figure 6.** Density maps for the lateral (top) and front (bottom) views in Benabid's stereotactic reference space. The plane is divided into  $0.01\text{-mm}^2$  squares, and 22 individual maps are superimposed. A density of 1 means that the 22 corresponding squares are included in the MRI anatomy-based polygons for all the 22 subjects. A density of 0.5 means that the corresponding squares were included in the MRI anatomy-based polygons for 11 subjects. Density maps are displayed using grayscale from black = 0 to white = 1.

## DISCUSSION

The results show that STN stereotactic AC-PC-based diagrams are not perfectly representative of the STN, at least as determined on MRI. The MRI-localized STN tends to be located more posteriorly and medially than the probabilistic location proposed by stereotactic ACPC-based diagrams. Thus, any definitive conclusions on the best method of primary targeting, i.e., indirect or direct, based on retrospective analysis of target location relatively to the best DBS electrode contact, should be interpreted with caution (see Introduction) because the two methods do not target the same structure. Stereotactic AC-PC-based diagrams are likely outlying, located closer to the optimal site of the electrode contact used in DBS for severe Parkinson's disease, and are situated in the superior and lateral region of the STN and/or nearby laterally and above [12–20].

Therefore, STN targeting, despite being widely used, should nevertheless be defined more precisely; hence 'dorsolateral STN subthalamic area' targeting (centered on the dorsolateral region of the STN and its subthalamic vicinity) would be more relevant and realistic. Regardless of whether primary targeting is indirect or direct, the common objective is to reach the precise region offering the best efficacy without severe adverse effects. Detailed knowledge of this region, over and above coordinates for surgical targeting, can be built by adding all pertinent data: intraoperative electrophysiological recordings, clinical assessments (during awake surgery and/or postoperatively) and anatomical location which is only definable *in vivo* by MRI anatomy scans.

### MRI FOR STN TARGETING IN STEREOTACTIC SURGERY

STN can be identified directly on MRI at 1.5 or 3 T, as reported by different teams [18, 23–28]. However, despite wide-scale routine use, the contribution of MRI to the task of targeting deep brain structures is still subject to debate [9–11, 29, 30]. Teams continue using MRI simply to determine AC-PC landmarks [13, 24, 31–33]. In parallel, several publications have shown that direct targeting of deep-situated nuclei is relevant and achievable. Initially used for targeting the internal globus pallidum [21, 34, 35], the technique was extended to STN targeting with good clinical results [9, 12, 36]. In parallel, many intermediate or combined techniques combining MRI-based and landmark-based techniques are in widespread use [14, 15, 37].

The use of MRI for stereotactic targeting of deep-situated brain structures must fulfill a number of conditions, including stereotactic compatibility, i.e., minimal distortion, in particular if a stereotactic frame is in place during imaging, and anatomical compatibility, i.e., optimal visualization of target anatomy (nuclei and/or WM). The distortion linked to the homogeneity of the magnetic field and the linearity of gradients has been widely reported [38–42] and needs to be minimized following institutional and manufacturer-led quality controls, although recent MR units are able to reduce this distortion. Prior to routine use, it is preferable to test MR sequences on a phantom, including the stereotactic frame [43]. The geometric accuracy of images is one element of the whole surgical chain influencing the placement of DBS electrodes or lesioning. Other relevant factors include stereotactic system (with frame or frameless), calculation of coordinates and trajectory (manually or computer-aided) and several intraoperative pitfalls (brain shift, calibration of tools used to place an electrode, electrode fixation, frame repositioning), and intraoperative and postoperative imaging controls. In our study, the significant discordance between MRI-based STN location and AC-PC-based diagrams for any of the x, y or z coordinates must be modulated in terms of contouring accuracy. Contouring accuracy was limited by available voxel size,  $0.6 \times 0.5 \times 2 \text{ mm}^3$ , which was not isotropic and was therefore less accurate in the stereotactic y-axis. However, this voxel size is one of the most accurate used in this kind of study ( table 3 ).

| Author, year               | n  | MRI   | Voxel size, mm                | Acquisition plan         | Ref. point/analysis           | Side                  | Mean coordinates of geometrical center, mm          |  |  |
|----------------------------|----|-------|-------------------------------|--------------------------|-------------------------------|-----------------------|---|--|--|
|                            |    |       |                               |                          |                               |                       | x   | y/ref.   | z  |
| Zhu et al. [57], 2002      | 35 | 1.5 T | n.a. $\times$ n.a. $\times$ 3 | axial                    | geometrical center/n.a.       | right<br>left         | $12.7 \pm 1.3$<br>$12.59 \pm 1.43$                  | n.a.   | n.a.   |
| Richter et al. [56], 2004  | 18 | 1.5 T | $1.05 \times 1.05 \times 2$   | axial, coronal           | geometric center/n.a.         | both                  | $12.2 \pm 0.9$                                      | $-3.8 \pm 1.3/\text{MidP}$   | $-5.1 \pm 0.7$                                       |
| Schlaier et al. [54], 2005 | 14 | 1.5 T | n.a. $\times$ n.a. $\times$ 3 | axial, coronal           | dorsolateral STN              | both                  | $10.75 \pm 0.94$ (axial)<br>$10 \pm 1.03$ (coronal) | $-1.26 \pm 1.06/\text{MidP}$ (axial)<br>$-1.1 \pm 1.5/\text{MidP}$ (coronal)           | $-6.65 \pm 1.5$ (axial)<br>$-5.9 \pm 1.43$ (coronal) |
| Danish et al. [53], 2006   | 26 | 1.5 T | $1.05 \times 1.05 \times 2.5$ | axial                    | center/n.a.                   | both                  | $10.0 \pm 0.7$                                      | $-0.2 \pm 0.7/\text{MidP}$   | $-3.3 \pm 0.9$                                       |
| Slavin et al. [27], 2006   | 13 | 3 T   | $0.5 \times 0.5 \times 1.5$   | axial, coronal, sagittal | center/2D                     | left<br>right         | $11.4 \pm 1.3$<br>$11.5 \pm 0.9$                    | $-1.1 \pm 2.3/\text{MidP}$<br>$-0.6 \pm 1.8/\text{MidP}$                               | $-4.7 \pm 1.9$<br>$-5.0 \pm 1.7$                     |
| Ashkan et al. [55], 2007   | 29 | 1.5 T | n.a. $\times$ n.a. $\times$ 2 | axial                    | 'within the STN' <sup>1</sup> | both                  | $10.3 \pm 1.3$                                      | $-11.4 \pm 1.3/\text{AC}$  | $-4.7 \pm 1$   |
| This study                 | 22 | 1.5 T | $0.6 \times 0.6 \times 2$     | coronal                  | barycenter/3D                 | left<br>right<br>both | $9.2 \pm 1.3$<br>$9.08 \pm 1.3$<br>$9.1 \pm 1.3$    | $-2.5 \pm 0.9/\text{MidP}$<br>$-2.6 \pm 0.9/\text{MidP}$<br>$-2.6 \pm 0.9/\text{MidP}$ | $-3.14 \pm 1$<br>$-3.23 \pm 0.9$<br>$-3.2 \pm 0.9$   |

**Table 3.** Localization of STN geometrical centers on MRI. *n* = Number of STN analyzed. <sup>1</sup> At a level of up to 1 mm in front of a line joining the anterior borders of the red nucleus on the scan showing the largest diameter of the red nucleus.

MR sequences have to be optimized to improve the distinction between the STN and neighboring structures (thalamus, zona incerta, Forel's field, SN, pyramidal tract, ansa lenticularis and its nucleus, and red nucleus). The T2-weighted TSE sequence used in this study was optimized in our institution [unpubl. data]. Recent publications report promising dedicated sequences using an inversion recovery technique [18, 44, 45].

Even with optimal MRI sequence quality, advanced anatomical knowledge is still necessary in order to identify the different deep-located structures, particularly in the subthalamic region [23–27, 46–49]. Stereotactic atlases can also be useful for pinpointing the STN, providing an anatomical aid to identify the STN from among the other diencephalic and/or mesencephalic structures, and practically any anatomic textbook can be used as long as it offers original detailed information. However, the main limitations of classical atlases and anatomic textbooks are that users are limited to a few section (slice) orientations and tend not to rely on detailed MRI-based anatomy. In our institution, we have at our disposal highfield MR images of an anatomic specimen (4.7 T, voxel size = 0.253 mm<sup>3</sup>) which is used as a reference atlas for visual recognition of deep cerebral structures [50], and other authors have begun to follow similar procedures [51].

Finally, the correspondence between MRI-based STN identification and intraoperative assessments (clinical tests and microrecordings; performed during the secondary targeting step focusing on the optimal site for electrode contact positioning in severe Parkinson's disease) has been documented as reliable [18, 22], in agreement with another study exploring MRI anatomy and electrophysiology [52].

### MRI-BASED STN LOCATION

There are limited literature data on the anatomical STN localization on MR images [27, 53–57] (table 3). When based strictly on coordinate values, the results are tangibly different. Compared with our data, the largest difference is 3.6 mm on the x-axis, 2.6 mm on the y-axis and –1.9 mm on the y-axis. On the other hand, Danish et al. [53] posted results close to ours, except for the y-axis. However, comparisons have to be taken with care due to obvious differences in terms of voxel size, slice orientation (which strongly influences the identification of the STN) and definition of the STN 'center'. Interestingly, Schlaier et al. [54] comparing MRI with atlas-based

STN locations arrived at almost the same conclusion as we did, *i.e.*, (a) atlas-derived STN coordinates are located more laterally and dorsally; (b) the anterior-posterior difference is linked to slice orientation, as atlas-based coordinates are more anterior on axial slices and more posterior on coronal slices, which may be directly linked to the fact that atlases use different anatomic specimens for each section plane. Only Acar et al. [24] concluded that there are no significant differences between AC-PC-based and MRI anatomy-based STN locations (no coordinate values available), but the differences (no information on direction) on the x-, y- and z-axes ranged from 0 to 1.1, from 0.1 to 2, and from 0 to 1.9 mm, respectively.

## CONCLUSION

The STN can be identified on dedicated MR images, allowing reliable contouring of its boundaries. Comparisons with routine AC-PC-based stereotactic diagrams exhibited systematic differences, as MR images show the STN as more posterior, medial and slightly inferior. The coordinates of the STN CG were as follows:  $x = 9.1 \pm 1.3$  mm,  $y = 2.6 \pm 0.9$  mm from MidP, and  $z = -3.2 \pm 0.97$  mm.

These results do not reappraise the specific value or safety of any particular indirect or direct targeting method for functional surgery. Our aim was to clarify anatomo-functional relationships for each individual, especially as there is significant interindividual variability in STN shape and location [28]. The main conclusions for clinical practice are: (a) preoperatively, a most precise definition of a surgical anatomic target according to MRI anatomy, *i.e.*, the so-called ‘STN targeting’, is confusing since ‘dorsolateral STN subthalamic area’ targeting is likely more appropriate; (b) postoperatively, more precise anatomic location of effective contacts, and consequently, better interpretation of DBS mechanisms. Our results also allow confirming that the center of the STN is not the optimal target for the standard DBS during severe Parkinson’s disease.

Furthermore, of interest for teams using indirect targeting is that this study is the first attempt to give a probabilistic representation of frontal and lateral STN projections in a routine AC-PC frame, based on the normalization of a frequentist approach. Our approach could be extended

with volumetric data, allowing a 3-dimensional representation of the STN instead of simple front and lateral projections.

## REFERENCES

- 1 Talairach J, David M, Tournoux P, et al: Atlas d'anatomie stéréotaxique. Repérage radiologique indirect des noyaux gris centraux des régions mésencéphalo-sous-optiques et hypothalamiques de l'homme. Paris, Masson et Cie, 1957.
- 2 Benabid AL, Koudsie A, Benazzouz A, Le Bas JF, Pollak P: Imaging of subthalamic nucleus and ventralis intermedius of the thalamus. *Mov Disord* 2002;17(suppl 3):S123–S129.
- 3 Schaltenbrand G, Bailey P: Introduction to stereotaxis with an atlas of the human brain vol 2. Stuttgart, Thieme, 1959.
- 4 Nowinski WL, Thirunavuukarasuu A, Benabid AL: The Cerefy Clinical Brain Atlas. Stuttgart, Thieme, 2004.
- 5 Nowinski WL, Belov D, Pollak P, Benabid AL: Statistical analysis of 168 bilateral subthalamic nucleus implantations by means of the probabilistic functional atlas. *Neurosurgery* 2005;57(4 Suppl):319–330.
- 6 Bardinet E, Bhattacharjee M, Dormont D, Pidoux B, Malandain G, Schüpbach M, Ayache N, Cornu P, Agid Y, Yelnik J: A threedimensional histological atlas of the human basal ganglia. 2. Atlas deformation strategy and evaluation in deep brain stimulation for Parkinson disease. *J Neurosurg* 2009;110: 208–219.
- 7 Stancanello J, Muacevic A, Sebastiano F, Modugno N, Cerviri P, Ferrigno G, Uggeri F, Romanelli P: 3T MRI evaluation of the accuracy of atlas-based subthalamic nucleus identification. *Med Phys* 2008;35:3069–3077.
- 8 Andrade-Souza YM, Schwalb JM, Hamani C, Eltahawy H, Hoque T, Saint-Cyr J, Lozano AM: Comparison of three methods of targeting the subthalamic nucleus for chronic stimulation in Parkinson's disease. *Neurosurgery* 2008;62(suppl 2):875–883.
- 9 Lemaire JJ, Coste J, Ouchchane L, Caire F, Nuti C, Derost P, Cristini V, Gabrillargues J, Hemm S, Durif F, Chazal J: Brain mapping in stereotactic surgery: a brief overview from the probabilistic targeting to the patientbased anatomic mapping. *Neuroimage* 2007; 37(suppl 1):S109–S115.

- 10 Breit S, LeBas JF, Kouksie A, Schulz J, Benazzouz A, Pollak P, Benabid AL: Pretargeting for the implantation of stimulation electrodes into the subthalamic nucleus: a comparative study of magnetic resonance imaging and ventriculography. *Neurosurgery* 2006;58(suppl 1):ONS83–ONS95.
- 11 Cuny E, Guehl D, Burbaud P, Gross C, Dousset V, Rougier A: Lack of agreement between direct magnetic resonance imaging and statistical determination of a subthalamic target: the role of electrophysiological guidance. *J Neurosurg* 2002;97:591–597.
- 12 Saint-Cyr JA, Hoque T, Pereira LC, Dostrovsky JO, Hutchison WD, Mikulis DJ, Abosch A, Sime E, Lang AE, Lozano AM: Localization of clinically effective stimulating electrodes in the human subthalamic nucleus on magnetic resonance imaging. *J Neurosurg* 2002;97:1152–1166.
- 13 Lanotte MM, Rizzone M, Bergamasco B, Faccani G, Melcarne A, Lopiano L: Deep brain stimulation of the subthalamic nucleus: anatomical, neurophysiological, and outcome correlations with the effects of stimulation. *J Neurol Neurosurg Psychiatry* 2002; 72:53–58.
- 14 Voges J, Volkmann J, Allert N, Lehrke R, Koulousakis A, Freund HJ, Sturm V: Bilateral high-frequency stimulation in the subthalamic nucleus for the treatment of Parkinson disease: correlation of therapeutic effect with anatomical electrode position. *J Neurosurg* 2002;96:269–279.
- 15 Hamel W, Fietzek U, Morsnowski A, Schrader B, Herzog J, Weinert D, Pfister G, Muller D, Volkmann J, Deuschl G, Mehdorn HM: Deep brain stimulation of the subthalamic nucleus in Parkinson's disease: evaluation of active electrode contacts. *J Neurol Neurosurg Psychiatry* 2003;74:1036–1046.
- 16 Herzog J, Fietzek U, Hamel W, Morsnowski A, Steigerwald F, Schrader B, Weinert D, Pfister G, Müller D, Mehdorn HM, Deuschl G, Volkmann J: Most effective stimulation site in subthalamic deep brain stimulation for Parkinson's disease. *Mov Disord* 2004;19: 1050–1054.
- 17 Godinho F, Thobois S, Magnin M, Guenot M, Polo G, Benatru I, Xie J, Salvetti A, Garcia-Larrea L, Broussolle E, Mertens P: Subthalamic nucleus stimulation in Parkinson's disease: anatomical and electrophysiological localization of active contacts. *J Neurol* 2006; 253:1347–1355.
- 18 Lemaire JJ, Coste J, Ouchchane L, Hemm S, Derost P, Ulla M, Siadoux S, Gabrillargues J, Durif F, Chazal J: MRI anatomical mapping and direct stereotactic targeting in the subthalamic region: functional and anatomical correspondence in Parkinson's disease. *Int J CARS* 2007;2:75–85.

- 19 McClelland S 3rd, Vonsattel JP, Garcia RE, Amaya MD, Winfield LM, Pullman SL, Yu Q, Fahn S, Ford B, Goodman RR: Relationship of clinical efficacy to postmortem-determined anatomic subthalamic stimulation in Parkinson syndrome. *Clin Neuropathol* 2007;26:267–275.
- 20 Sun DA, Yu H, Spooner J, Tatsas AD, Davis T, Abel TW, Kao C, Konrad PE: Postmortem analysis following 71 months of deep brain stimulation of the subthalamic nucleus for Parkinson disease. *J Neurosurg* 2008;109: 325–329.
- 21 Lemaire JJ, Durif F, Boire JY, Debilly B, Irthum B, Chazal J: Direct stereotactic MRI location in the globus pallidus for chronic stimulation in Parkinson’s disease. *Acta Neurochir* 1999;141:759–766.
- 22 Coste J, Ouchchane L, Sarry L, Derost P, Durif F, Gabrillargues J, Hemm S, Lemaire JJ: New electrophysiological mapping combined with MRI in parkinsonian’s subthalamic region. *Eur J Neurosci* 2009;29:1627–1633.
- 23 Bejjani BP, Dormont D, Pidoux B, Yelnik J, Damier P, Arnulf I, Bonnet AM, Marsault C, Agid Y, Philippon J, Cornu P: Bilateral subthalamic stimulation for Parkinson’s disease by using three-dimensional stereotactic magnetic resonance imaging and electrophysiological guidance. *J Neurosurg* 2000;92:615–625.
- 24 Acar F, Miller JP, Berk MC, Anderson G, Burchiel KJ: Safety of anterior commissureposterior commissure-based target calculation of the subthalamic nucleus in functional stereotactic procedures. *Stereotact Funct Neurosurg* 2007;85:287–291.
- 25 Pollo C, Meuli R, Maeder P, Vingerhoets F, Ghika J, Villemure JG: STN DBS for Parkinson’s disease: MRI targeting using visible anatomical landmarks. *Stereotact Funct Neurosurg* 2003;80:76–81.
- 26 Giller CA, Babcock EE, Mendelsohn DB: Use of sagittal images for localization of the subthalamic nucleus. Technical note. *J Neurosurg* 2005;102:571–575.
- 27 Slavin KV, Thulborn KR, Wess C, Nersesyan H: Direct visualization of the human subthalamic nucleus with 3T MR imaging. *AJNR Am J Neuroradiol* 2006;27:80–84.
- 28 Patel NK, Khan S, Gill SS: Comparison of atlas- and magnetic-resonance-imaging-based stereotactic targeting of the subthalamic nucleus in the surgical treatment of Parkinson’s disease. *Stereotact Funct Neurosurg* 2008; 86:153–161.

- 29 Schuurman PR, de Bie RM, Majoie CB, Speelman JD, Bosch DA: A prospective comparison between three-dimensional magnetic resonance imaging and ventriculography for target-coordinate determination in frame-based functional stereotactic neurosurgery. *J Neurosurg* 1999;91:911–914.
- 30 Rezaï AR, Kopell BH, Gross RE, Vitek JL, Sharan AD, Limousin P, Benabid AL: Deep brain stimulation for Parkinson’s disease: surgical issues. *Mov Disord* 2006;21(suppl 14):S197–S218.
- 31 Starr PA, Vitek JL, DeLong M, Bakay RA: Magnetic resonance imaging-based stereotactic localization of the globus pallidus and subthalamic nucleus. *Neurosurgery* 1999; 44:303–313.
- 32 Sterio D, Zonenshayn M, Mogilner AY, Rezaï AR, Kiproviski K, Kelly PJ, Beric A: Neurophysiological refinement of subthalamic nucleus targeting. *Neurosurgery* 2002;50:58–67.
- 33 Zonenshayn M, Rezaï AR, Mogilner AY, Beric A, Sterio D, Kelly PJ: Comparison of anatomic and neurophysiological methods for subthalamic nucleus targeting. *Neurosurgery* 2000;47:282–292.
- 34 Vayssière N, Hemm S, Zanca M, Picot MC, Bonafe A, Cif L, Frerebeau P, Coubes P: Magnetic resonance imaging stereotactic target localization for deep brain stimulation in dystonic children. *J Neurosurg* 2000;93:784–790.
- 35 Vayssi re N, Hemm S, Cif L, Picot MC, Diakonova N, El Fertit H, Frerebeau P, Coubes P: Comparison of atlas- and magnetic resonance imaging-based stereotactic targeting of the globus pallidus internus in the performance of deep brain stimulation for treatment of dystonia. *J Neurosurg* 2002;96:673–679.
- 36 Derost PP, Ouchchane L, Morand D, Ulla M, Llorca PM, Barget M, Debilly B, Lemaire JJ, Durif F: Is DBS-STN appropriate to treat severe Parkinson disease in an elderly population? *Neurology* 2007;68:1345–1355.
- 37 Starr PA, Christine CW, Theodosopoulos PV, Lindsey N, Byrd D, Mosley A, Marks WJ Jr: Implantation of deep brain stimulators into the subthalamic nucleus: technical approach and magnetic resonance imaging-verified lead locations. *J Neurosurg* 2002;97: 370–387.
- 38 Sumanaweera TS, Adler JR Jr, Napel S, Glover GH: Characterization of spatial distortion in magnetic resonance imaging and its implications for stereotactic surgery. *Neurosurgery* 1994;35:696–703.
- 39 Sumanaweera T, Glover G, Song S, Adler J, Napel S: Quantifying MRI geometric distortion in tissue. *Magn Reson Med* 1994;31:40–47.

- 40 Walton L, Hampshire A, Forster DM, Kemeny AA: Stereotactic localization using magnetic resonance imaging. *Stereotact Funct Neurosurg* 1995;64(suppl 1):155–163.
- 41 Walton L, Hampshire A, Forster DM, Kemeny AA: A phantom study to assess the accuracy of stereotactic localization, using T1-weighted magnetic resonance imaging with the Leksell stereotactic system. *Neurosurgery* 1996;38:170–176.
- 42 Burchiel KJ, Nguyen TT, Coombs BD, Szumoski J: MRI distortion and stereotactic neurosurgery using the Cosman-RobertsWells and Leksell frames. *Stereotact Funct Neurosurg* 1996;66:123–136.
- 43 Bourgeois G, Magnin M, Morel A, Sartoretti S, Huisman T, Tuncdogan E, Meier D, Jeanmonod D: Accuracy of MRI-guided stereotactic thalamic functional neurosurgery. *Neuroradiology* 1999;41:636–645.
- 44 Magnotta VA, Gold S, Andreasen NC, Ehrhardt JC, Yuh WT: Visualization of subthalamic nuclei with cortex attenuated inversion recovery MR imaging. *Neuroimage* 2000;11:341–346.
- 45 Hariz MI, Krack P, Melvill R, Jorgensen JV, Hamel W, Hirabayashi H, Lenders M, Wesslen N, Tengvar M, Yousry TA: A quick and universal method for stereotactic visualization of the subthalamic nucleus before and after implantation of deep brain stimulation electrodes. *Stereotact Funct Neurosurg* 2003;80:96–101.
- 46 Dormont D, Ricciardi KG, Tande D, Parain K, Menuel C, Galanaud D, Navarro S, Cornu P, Agid Y, Yelnik J: Is the subthalamic nucleus hypointense on T2-weighted images? A correlation study using MR imaging and stereotactic atlas data. *AJNR Am J Neuroradiol* 2004;25:1516–1523.
- 47 Lee C, Young B, Sanders MF: The role of the supramammillary commissure in MR localization of the subthalamic nucleus. *Stereotact Funct Neurosurg* 2006;84:193–204.
- 48 Caire F, Derost P, Coste J, Bonny JM, Durif F, Frenoux E, Villeger A, Lemaire JJ: Stimulation sous-thalamique dans la maladie de Parkinson idiopathique: étude de la localisation des contacts effectifs. *Neurochirurgie* 2006;52:15–25.